Polarized triton elastic scattering at 17 MeV

R. A. Hardekopf, R. F. Haglund, Jr., G. G. Ohlsen, W. J. Thompson,* and L. R. Veeser
Los Alamos Scientific Laboratory, University of California, Los Alamos, New Mexico 87545
(Received 19 June 1979)

We present differential-cross-section and analyzing-power angular distributions for the elastic scattering of polarized tritons from 13 nuclei with $40 \leq A \leq 208$. Data obtained at an energy of 17 MeV and in the angular range $20° \leq \theta \leq 160°$ are the basis for an optical-model analysis in which parameters which fit both observables simultaneously are determined. It is observed that the analyzing-power data delimit the real potential well parameters much more precisely than do cross-section data alone. Although the spin-orbit potential is less well defined, the average spin-orbit well depth is $V_{so} = 6.2 \pm 1.5$ MeV with geometry parameters similar to those for nucleons. The spin-orbit volume integrals are about a factor of 3 greater than predicted from simple folding models.

[NUCLEAR REACTIONS ^{40}Ca, ^{46}Ti, ^{48}Ti, ^{54}Fe, ^{56}Fe, ^{58}Ni, ^{60}Ni, ^{68}Zn, ^{90}Zr, ^{94}Zr, ^{116}Sn, ^{140}Ce, ^{208}Pb(t,t), $E = 17$ MeV; measured $\sigma(\theta)$, $A_y(\theta)$; optical-model analysis.]

I. INTRODUCTION

The nuclear optical model (OM) is useful in parametrizing elastic scattering data when there are no significant compound-nucleus effects. The potential parameters thus obtained give information on the macroscopic scattering interaction between nuclei and condense a large body of data to manageable proportions. Parameters that vary smoothly with mass number and energy permit interpolation to regions where data do not exist, and wave functions obtained from such parameter sets are often used in distorted-wave Born approximation (DWBA) calculations for reactions.

Unfortunately, the optical model is fraught with ambiguities, and obtaining consistent parameters from many different data sets and analyses has proved to be difficult, particularly for composite projectiles such as deuterons, tritons, and helions (^{3}He nuclei) where a lack of sufficient data has added to the difficulty. For nucleon-nucleus scattering, these ambiguities were essentially solved when polarization data became available, thus allowing the determination of the spin-orbit potential for proton scattering. Refinements of the double scattering techniques used in the earliest measurements and the advent of polarized ion sources eventually resulted in a large body of polarization data for protons. Analyses of both cross section and polarization observables have produced several global sets of parameters that accurately describe nucleon elastic scattering for a wide range of energies and target masses.[1]

The ambiguities of the optical model for triton and helion scattering have not yet been systematically investigated. One reason is that these composite projectiles are strongly absorbed, so that determination of the strength and type of absorptive potential becomes a critical problem. Experimental difficulties have also hindered the acquisition of extensive polarization data. Double-scattering techniques which worked well for nucleons proved difficult for composite projectiles, complicated by the spin-1 nature of the deuteron and the extremely small cross sections for mass-3 scattering at angles greater than 60°. Accurate and complete polarization data for these projectiles had to await the development of ion sources that could produce reasonable beam intensities of polarized composite projectiles.

Sources of polarized helions[2] and tritons[3] have only recently become available. Analyzing-power results for helions have been limited mainly to light nuclei and forward angles where counting rates are large enough, even with the small beam intensities achieved thus far. Nevertheless, enough data have been obtained on heavier nuclei to produce significant results in the search for helion OM parameters.[4] A preliminary report of polarized triton scattering at 15 MeV (Ref. 5) showed for the first time that the analyzing powers for scattering from medium weight nuclei, especially at angles larger than 90°, were much greater than predicted on the basis of simple theoretical arguments. The results from analyses of these triton data also showed important differences from the helion OM parameters, although direct comparison was not possible because of the different energies, targets, and angular range of the respective experiments. A comparison of triton and helion results for light target nuclei[6] suffered from the marginal applicability of the OM in this mass range.

The purpose of our experiment was to obtain a large enough body of data to allow a comprehensive study of the triton OM. Because of the many possible approaches to an OM analysis, we do not claim that our parameters are definitive. Indeed, it is anticipated that further analyses of these data will help to clarify many of the problems that we encountered. Nevertheless, in addition to the experimental data we provide the first study of the optical model for mass-3 projectiles that spans a large range of target masses ($40 \leq A \leq 208$) and scattering angles ($20° \leq \theta \leq 160°$) and includes both cross-section and analyzing-power data. The bombarding energy of 17 MeV was chosen because it is the highest energy we can consistently obtain with the polarized triton beam. Especially for the heaviest nuclei, the diffraction effects were small at the 15-MeV energy of our previous results, and the 2-MeV increase has increased these. In addition, most of the reactions initiated by polarized tritons have used 17-MeV incident energy, and thus our OM parameters will be applicable to such analyses.

II. EXPERIMENTAL METHOD

The measurements were made possible by the installation of a polarized triton source[3] on the Los Alamos Scientific Laboratory (LASL) tandem Van de Graaff accelerator. Beam intensities available at the target ranged from 20–60 nA during the 11 days of data acquisition, and beam polarization was 0.75–0.80. Because tritons are strongly absorbed, the differential cross section falls off sharply as a function of scattering angle; scattered intensities drop by 5 orders of magnitude from 20° to 160°, resulting in cross sections as small as 20 μb/sr at the largest angles. For various reasons it was impractical to use more than one target for each nucleus studied, but the thick targets required to attain sufficient counting rates at the backward angles gave very high rates at forward angles and poor energy resolution, especially around 90°. Consequently, we limited target selection to those nuclei (see Table I) having a first-excited level at least 800 keV above the ground state to avoid including inelastically scattered tritons in the elastic spectra, and we kept the electronic dead time acceptable by reducing beam intensities at forward angles. Even so, we could not obtain reliable results for angles smaller than 20°.

The target and detectors were housed in a large, cubical vacuum chamber[7] especially designed for accurate polarization measurements. To keep the beam centered in both left-right and up-down directions, the beam currents on slits at the entrance and exit of the chamber were continuously monitored and kept balanced. A current integrator recorded the total charge accumulated on the exit slits and in an electrically suppressed Faraday cup behind them. The beam was focussed to a spot size approximately 2.0 mm square.

A mount at the center of the scattering chamber held the target foil either perpendicular to the beam or, for scattering angles near 90°, at a 45° angle. Two pairs of detector telescopes with angular resolutions of ±0.4° were mounted 15°

TABLE I. Characteristics of targets used in the experiment. Values in parentheses are estimates. The energy loss in the target is ΔE. The optical-model renormalizations are the values by which the measurements were multiplied, and were determined in the analysis by minimizing the χ_σ^2 values for $\theta \leq 40°$.

Target	Target thickness (mg/cm^2)	ΔE (MeV)	First-excited state (MeV)	Isotopic purity (%)	Optical-model renormalization
^{40}Ca	(5.0)	(0.24)	3.35	96.8	1.67
^{46}Ti	5.9	0.25	0.89	81.0	1.15
^{48}Ti	5.7	0.24	0.98	99.6	0.97
^{54}Fe	4.7	0.20	1.41	88.3	1.27
^{56}Fe	4.5	0.19	0.85	99.5	1.17
^{58}Ni	4.1	0.18	1.45	99.3	1.07
^{60}Ni	3.9	0.17	1.33	99.8	1.15
^{68}Zn	4.8	0.20	1.08	98.5	1.16
^{90}Zr	10.8	0.39	1.76	98.1	1.17
^{94}Zr	5.5	0.20	0.92	97.1	1.15
^{116}Sn	8.2	0.28	1.29	(98.0)	1.02
^{140}Ce	6.6	0.20	1.60	88.5	1.29
^{208}Pb	(3.0)	(0.08)	2.61	98.0	0.93

apart left and right of the beam axis. Each telescope consisted of a 300-μm-thick ΔE and a 1000-μm-thick E silicon surface-barrier detector. For events having a ΔE-E coincidence, linear signals were processed by analog-to-digital converters and stored in an on-line computer which was programmed for the mass identification and recording of triton pulse-height spectra. After we chose gates around an elastic peak, the computer estimated the background by finding a linear fit between a few channels in the valleys below and above the peak. For targets with relatively low first-excited states (see Table I) and for the middle angles, $70° \leq \theta \leq 110°$, where we used the 45° target orientation, spectral broadening from triton energy losses in the target made proper peak integration imprecise, particularly for detectors facing the side of the target struck by the incident beam. Often during off-line re-analysis of such data we decided to use only the spectra from the telescope which detected tritons in the transmission mode; in these cases and others where the backgrounds were large or the peaks poorly defined, increased relative uncertainties were assigned accordingly.

The data acquisition sequence for each angle consisted of runs of equal integrated charge for triton-beam polarizations up and down. Beam polarization, determined several times each run by the quench-ratio technique, was maintained at 0.75–0.80 and was constant to within 0.01 during individual runs. The absolute calibration of the polarization is known[8] to within ±0.01. The calculation of the analyzing power A_y was made from the four peak sums (left and right detectors, up and down beam polarization) using standard techniques[9] which eliminate first-order errors due to current integration, target density, and detector solid-angle factors.

Energy losses in the targets ranged from 80 to 390 keV (see Table I). We adjusted the incident beam energy so that the energy at the center of each target was 17.0 ±0.1 MeV.

III. EXPERIMENTAL RESULTS

Table I lists the target nuclei studied along with other experimental information, and the data are shown in Figs. 1–5. We have tabulated the data in an informal report (LA-7863), which may be obtained by writing the authors.

For analyzing-power data, statistical errors ranged from less than 0.005 at forward angles to about 0.05 at the most backward angles. To account for random errors due to background determination and beam polarization fluctuations, we quadratically combined a systematic uncertainty of 0.01 with the statistical error to form the total error. Besides accounting for additional experimental uncertainties, this allowance for systematic error helped in the analysis by equalizing the weighting of the angular distribution between forward and backward angles; otherwise the forward angle data overly influence the re-

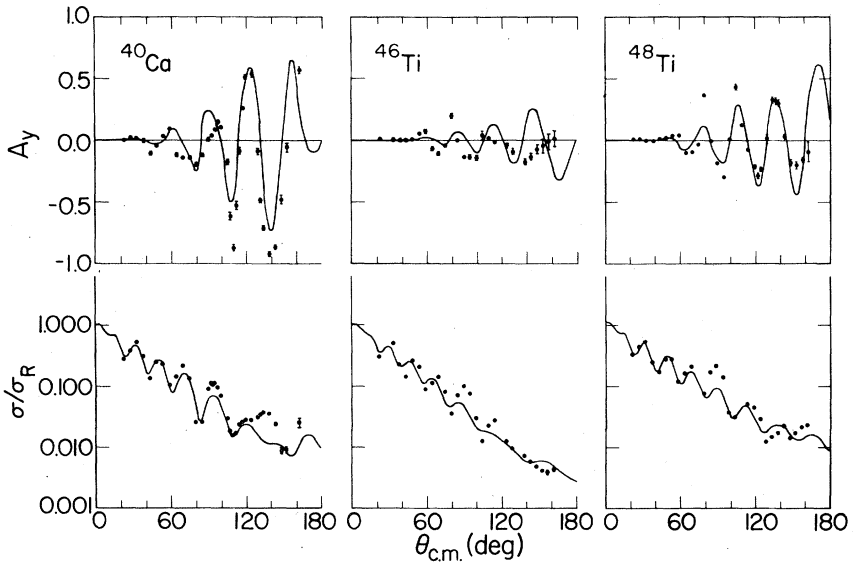

FIG. 1. The 17-MeV triton elastic scattering data for the three lightest nuclei studied, showing angular distributions of the analyzing powers A_y and differential cross sections σ/σ_R (ratio-to-Rutherford). The error bars are as shown or are smaller than the points. The curves shown are fits to the data using the parameters in Table II. The experimental cross sections have been renormalized according to Table I.

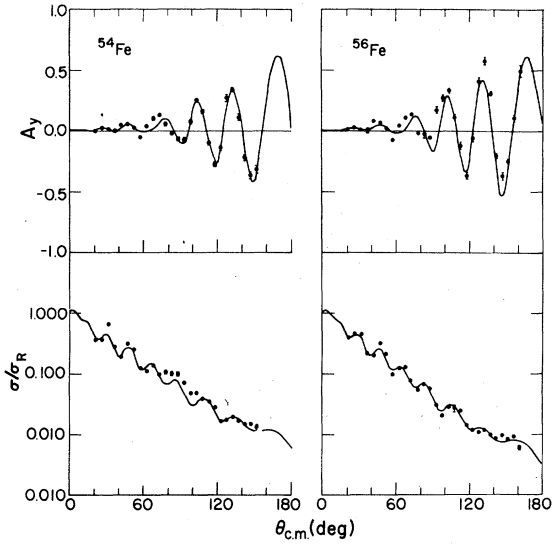

FIG. 2. Angular distributions of analyzing powers A_y and differential cross sections σ/σ_R for 17-MeV triton elastic scattering from the two iron isotopes studied. See caption for Fig. 1.

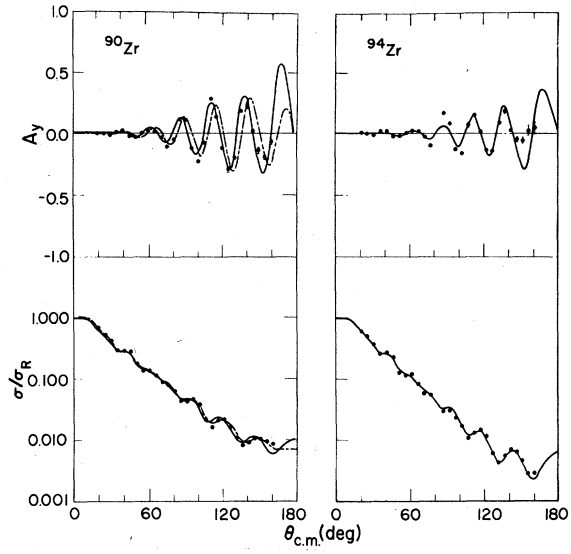

FIG. 4. Angular distributions of analyzing powers A_y and differential cross sections σ/σ_R for 17-MeV triton elastic scattering from the two zirconium isotopes studied. See caption for Fig. 1. The dashed curve for ^{90}Zr is an OM calculation with only V_0 changed, from the value in Table II, 165 MeV, to the value that gives the best fit to the cross-section data alone, 160 MeV.

sults of a χ^2-minimization search. The tabulated data include both statistical and total errors. The normalization of the analyzing-power data, determined from the quench-ratio beam polarization, is accurate to about ±1%.

For most of the differential cross-section data the statistical uncertainties in the numbers of counts are small, and other factors are believed to dominate the relative errors. Based on our estimate of the reliability of the current integration and dead-time corrections, relative solid angles, target uniformity, and most importantly the quality of the spectra, we assign a relative error of 5% to most of the cross-section data. We took the uncertainty of the background determination to be 50%, and for those few cases where the background under the peak was greater

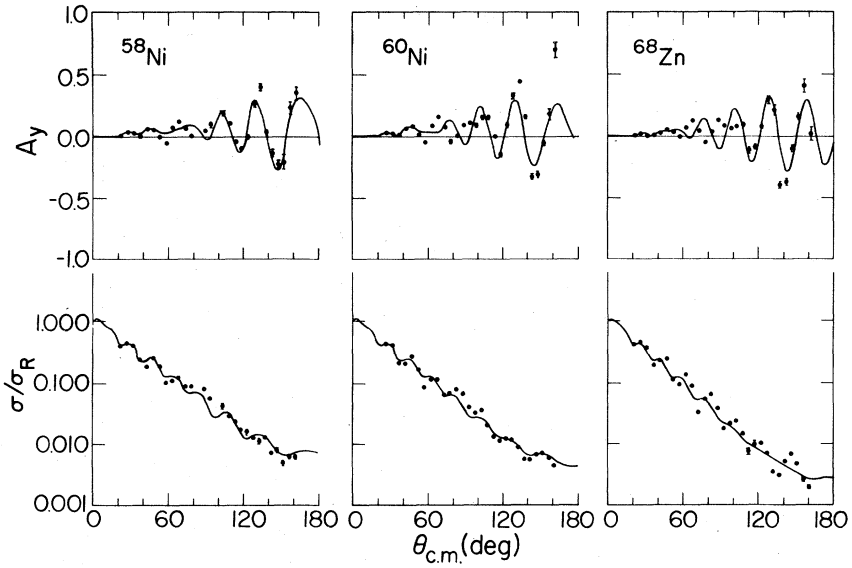

FIG. 3. Angular distributions of analyzing powers A_y and differential cross sections σ/σ_R for 17-MeV triton elastic scattering from the two nickel isotopes and ^{68}Zn. See caption for Fig. 1.

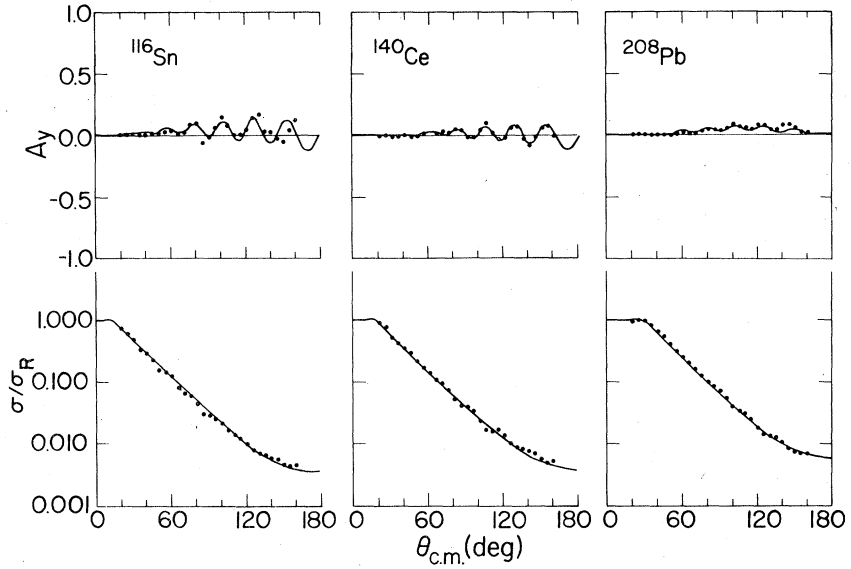

FIG. 5. Angular distributions of analyzing powers A_y and differential cross sections σ/σ_R for 17-MeV triton elastic scattering from the three heaviest nuclei studied. See caption for Fig. 1.

than 10% of the peak sum we increased the relative error accordingly.

Rough normalizations for the differential cross sections were made by either measuring or estimating the target thicknesses and calculating the absolute cross sections based on the experimental geometry. Because the uncertainties in this procedure can be large (the target uniformity and thicknesses were known only to about 20%), we allowed the overall normalizations of the cross section to vary during the fitting procedure, renormalizing our data to fit the OM calculations for $\theta \leq 40°$ where the cross section is dominated by Rutherford scattering and is relatively insensitive to the OM parameters.[10] Since our data do not extend to angles less than 20°, this procedure is not as reliable as in the analysis of Ref. 10, and we thus assign a normalization uncertainty of ±10%.

IV. OPTICAL-MODEL ANALYSIS

A. Computer codes

Two methods were used in the OM data analysis. First, we adapted the code OPTICS (Ref. 11) to run in an interactive mode on the MODCOMP data-acquisition computer at the LASL Van de Graaff Facility. The on-line display facilitated changes in calculation parameters and enabled grid scanning of a wide range of parameter values. Although this "directed" grid search was often more effective than steepest-descent ("automatic") searches in the early stages of the analysis, we added an automatic search as well, which proved useful in conjunction with the interactive parameter changes and on-line display. For more extensive parameter-grid calculations and automatic searches we used the code SNOOPY 3 (Ref. 12) on a CDC-6600 computer at LASL. Both codes use a standard OM parametrization with a potential of the form

$$U(r) = -V_0 f(r, r_0, a_0) - iW_v f(r, r_w, a_w) - V_{so}\frac{2}{r}\frac{d}{dr}[f(r, r_{so}, a_{so})]\vec{L}\cdot\vec{s} + V_C(r, r_C), \quad (1)$$

where the Woods-Saxon form factor

$$f(r, r_j, a_j) = 1\Big/\left[1 + \exp\left(\frac{r - r_j A^{1/3}}{a_j}\right)\right]. \quad (2)$$

Here A is the target mass, $\vec{s}$ is the projectile spin operator (magnitude $\frac{1}{2}$ for tritons), $\vec{L}$ is the orbital angular momentum operator, and $V_C(r, r_C)$ is the Coulomb potential for a uniformly charged sphere of radius $r_c A^{1/3}$. The factor 2 in the expression for the spin-orbit term is numerically equal to the pion Compton wavelength (in fm) squared, an artifact of the historical derivation of this potential from the Thomas form factor.

We used an error-weighted χ^2 function as a measure of the quality of the OM fits to the data and divided cross-section and analyzing-power χ^2 values by the number of data in the distributions to get the values shown in Table II. The cross-section χ^2 is

$$\chi_\sigma^2 = \frac{1}{N}\sum_{i=1}^{N}\left[\frac{\sigma_{OM}(\theta_i) - \sigma_{exp}(\theta_i)}{\Delta\sigma_{exp}(\theta_i)}\right]^2, \quad (3)$$

with a similar expression for the analyzing-power χ^2, $\chi_A{}^2$. The total χ^2, $\chi_T{}^2$, is the average of $\chi_\sigma{}^2$ and $\chi_A{}^2$. For automatic searches, the cross-section and analyzing-power distributions were weighted equally. Where several fits were found with nearly equal $\chi_T{}^2$, we preferred the one that gave the best visual fit to the data. For example, in the lighter nuclei it was often impossible to get the calculated analyzing power oscillations in phase with the data at both forward and backward angles. Since the oscillations at backward angles are much more pronounced, we usually matched the calculated and experimental phases in that region at the expense of the forward angle fit, particularly when the forward-angle analyzing-power data did not show a regular pattern of oscillations.

B. Starting potential sets; folding model

For starting values in the parameter searches, we looked to previous analyses of differential cross section data and to the predications of the folding model.

The first differential cross-section data for triton scattering suitable for OM analysis were those of Glover and Jones[13] at Aldermaston, who studied several nuclei with $A \leq 40$ at 12 MeV. Soon afterward, Hafele, Flynn, and Blair[14] at Los Alamos obtained 15- and 20-MeV cross-section data on heavier nuclei, and Flynn *et al.*[10] extended these results in mass number and angular range and included an OM analysis which we denote by FABB. The Los Alamos data have also been used in several subsequent OM studies of triton elastic scattering. Urone *et al.*[15] compare the ^{3}He and t potentials, in particular studying the isospin dependence. Mukhopadhyay, Srivastava, and Ganguly[16] (MSG) concluded from a microscopic analysis that a real well depth of around 125 MeV was the most physical and performed a phenomenological analysis from this starting point, and Nurzynski[17] re-analyzed the FABB data using a surface-absorption term in the optical potential instead of the more generally used volume absorption. Perhaps the most comprehensive study was the global analysis by Becchetti and Greenlees[18] (BG), who also used the FABB data set. They derived both energy- and isospin-dependent potentials that fit all of the cross-section data for $A \geq 40$ using real depths in the range of 150 MeV and volume absorption. In most of these cross-section analyses the spin-orbit potential was either ignored or set equal to a theoretical estimate of about 2 MeV.

Several authors have studied the folding model for composite-projectile OM potentials,[19-22] and most of the phenomenological analyses mentioned above used at least some of its predictions, either as starting values or as constraints on the parameter space explored. In the simplest application of the model to triton scattering the interaction between the triton and nucleus is assumed to be adiabatic and the nucleon-nucleus optical potential for each of the three nucleons is averaged over the internal motion of the triton. Such calculations show that the triton potential can be approximated by Woods-Saxon well shapes with V_0 about 3 times the nucleon well depth, and V_{so} about $\frac{1}{3}$ the nucleon spin-orbit well depth.[20,21] Absorption channels (such as breakup) which are open to the triton but not to nucleons are not properly accounted for by this model, so that predictions for the imaginary potential are not considered reliable. (See the review by Keaton[22] of OM calculations for deuterons, tritons, and helions.)

Attempts to obtain OM fits to the first available analyzing-power data for triton scattering at 15 MeV (Ref. 5) led to the surprising result that a spin-orbit potential about 3 times the folding-model prediction, that is, $V_{so} \cong 6$ MeV, was most consistent with the data, as shown in Fig. 2 of Ref. 5. Since a strong correlation between V_{so} and W_v was evident, and since the data covered only a few nuclei at a single energy, these findings were not felt to be conclusive. Other investigators believed that the folding-model estimates, $V_{so} \approx 2$ MeV, could be retained by invoking two-step contributions to the scattering.[23] It appears that the problem is too complicated to be answered by calculational models alone and that the proper OM potentials can be found only by analysis of a large body of data spanning many nuclei at several energies. In this paper we present one approach in the expectation that subsequent analyses will explore other avenues.

C. Analysis of ^{90}Zr

We began our analysis by studying the closed-shell nuclei ^{40}Ca, ^{90}Zr, ^{140}Ce, and ^{208}Pb where the effects of collective excitations are minimized. Of these, we chose ^{90}Zr as a medium-A nucleus with moderate sensitivity to the optical parameters and with uniformly accurate data for $20° \leq \theta \leq 160°$. This nucleus had also been included in all of the previous analyses of differential cross sections and in the preliminary analyzing-power results[5] at 15 MeV. To delimit the OM parameter space, we made grid searches on all the parameters for ^{90}Zr$(t, t)^{90}$Zr at 17 MeV,

and we investigated the sensitivity of χ_σ^2 and χ_A^2 to the OM parameters by using the interactive program and on-line display. For completeness and as a guide to future OM analyses we describe the search procedure in some detail.

First, we analyzed the differential cross section by making grid searches with initial parameter values from BG (Ref. 18) and with variations of at least 10% from these values for each parameter. Initially we held r_0, a_0, r_c and the spin-orbit parameters fixed ($V_{so}=2.5$ MeV from BG) and searched on V_0, W_v, r_w, and a_w to find χ_σ^2 minima and to examine the parameter dependence of the cross-section angular distributions. Eventually we varied a_0 in the search and investigated the ambiguity between V_0 and r_0. As expected,[24] we found that the cross section depends mainly on the real volume integral J_v [see Eq. (5)] rather than on the independent values of V_0 and r_0. Since values of r_0 near 1.20 fm (the BG value) gave good fits, we kept $r_0=1.20$ fm for ^{90}Zr. Later we reached a similar conclusion for each of the other target nuclei studied; thus $r_0=1.20$ fm became a fixed parameter of the analysis.

The next step of the ^{90}Zr analysis was to search for parameter sets giving an optimal fit to both analyzing-power and cross-section angular distributions. Here we held the real central potential fixed at the best-fit values for cross section alone and made grid searches on $V_{so}(2 \leq V_{so} \leq 12$ MeV), $r_{so}(0.6 \leq r_{so} \leq 1.4$ fm), $a_{so}(0.2 \leq a_{so} \leq 0.8$ fm), and $W_v(10 \leq W_v \leq 17$ MeV). The cross section at backward angles is sensitive to V_{so} because an increase of V_{so} fills in the diffraction minima since the diffraction patterns from the positive- and negative-polarization components become increasingly separated in angle as V_{so} increases. The analyzing power is sensitive to the central potential (both real and imaginary terms), mildly sensitive to r_{so} and a_{so}, and V_{so} acts approximately as an overall scale factor if all other parameters are fixed. Figure 6, which shows χ_A^2 contours for variations of V_0 and r_{so}, illustrates this sensitivity of the A_y data to V_0. It is seen that, because of the strong effect of the real volume integral on the phase of the A_y oscillation pattern, a 1% change in V_0, e.g., from 165 to 166.5 MeV, will double χ_A^2 while 25% changes in r_{so} have little effect.

We also observed that the χ_σ^2 and χ_A^2 contours generally do not exhibit minima for the same parameter values, so one must compromise between optimizing either the cross section or the analyzing-power fit. Figure 7 illustrates this for the strongly correlated parameters W_v and V_{so}. Not only are the χ^2 minima for these two observables separated (primarily in W_v), but the calculated analyzing power is much more sensitive to the absorption parameter than is the cross section. Hence, although the cross-section fits are sometimes poorer than those obtained in previous analyses for which analyzing-power data were not available, the polarized-beam measurements strongly constrain the acceptable central-potential parameters.

From these searches, we settled on a ^{90}Zr OM parametrization from which we would explore other ambiguities. We designate these the ZR1 parameters:

$$\begin{aligned} V_0&=165.0 \text{ MeV}, & W_v&=13.8 \text{ MeV}, & V_{so}&=6.0 \text{ MeV},\\ r_0&=1.20 \text{ fm}, & r_w&=1.60 \text{ fm}, & r_{so}&=1.10 \text{ fm},\\ a_0&=0.66 \text{ fm}, & a_w&=0.80 \text{ fm}, & a_{so}&=0.40 \text{ fm},\\ r_c&=1.30 \text{ fm}. \end{aligned} \quad (4)$$

Since changes in the Coulomb radius r_c affected the calculations only slightly, it was kept fixed at 1.30 fm throughout the analysis. The solid curves in Fig. 4 for ^{90}Zr are for the ZR1 parameters.

To further investigate the effect of the (V_0, r_0) ambiguity and the different sensitivity of χ_σ^2 and χ_A^2 to these parameters, Fig. 8 shows χ_σ^2 and χ_A^2 plotted as a function of V_0 for three values of r_0. The discrete ambiguities, arising from different numbers of nodes of the scattering wave function in the potential well but similar asymptotic wave functions, are readily apparent; as r_0 increases from 1.16 to 1.24 fm, the χ^2 minima move toward

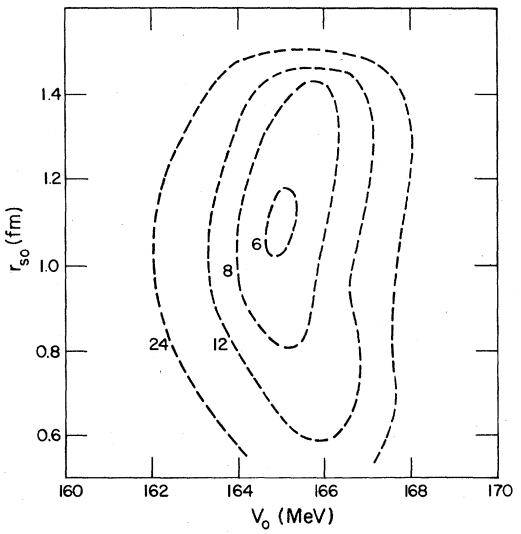

FIG. 6. Contours of χ_A^2 for ^{90}Zr$(t,t)^{90}$Zr are shown as a function of V_0 and r_{so} and illustrate the sensitivity of the analyzing power to the real central potential, while changes in the spin-orbit potential geometry have only a slight effect.

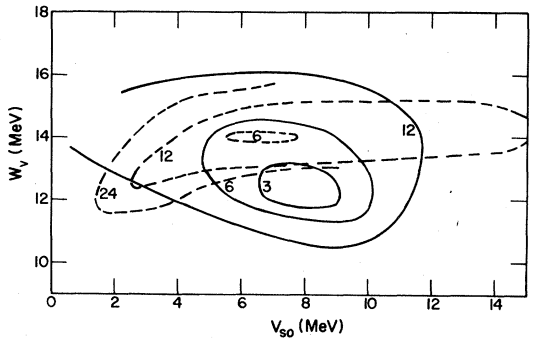

FIG. 7. Contours of χ_σ^2 (solid curves) and χ_A^2 (dashed curves) for $^{90}Zr(t,t)^{90}Zr$ as a function of V_{so} and W_v, showing that the minima for cross section and analyzing power often do not occur for the same values of the potential parameters. Also note the relative sensitivity of the analyzing power to W_v.

smaller values of V_0, maintaining roughly constant values of the real volume integral per nucleon[24];

$$J_v/A = \frac{4\pi V_0 R_0^3}{3A A_p}\left[1+\left(\frac{\pi a_0}{R_0}\right)^2\right]. \quad (5)$$

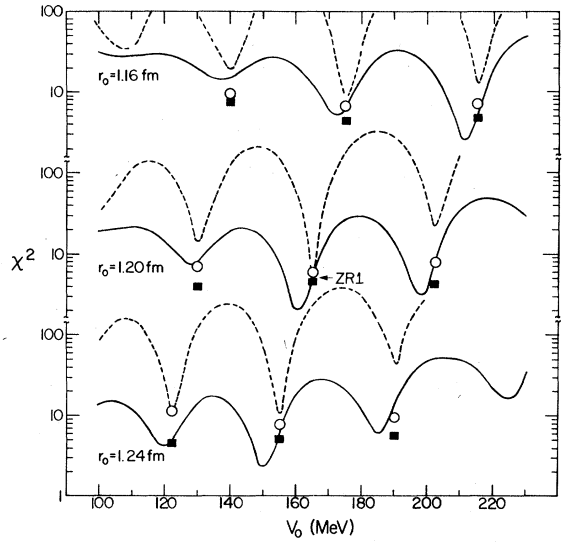

FIG. 8. Solid curves show χ_σ^2 and dashed curves show χ_A^2 for $^{90}Zr(t,t)^{90}Zr$ on a logarithmic scale as a function of V_0 for three values of r_0. The analyzing power displays sharper minima than the cross section, and χ_A^2 is displaced relative to χ_σ^2 in the direction of increasing V_0. Automatic searches at each χ_A^2 relative minimum produced the best-fit values indicated by squares for χ_σ^2 and circles for χ_A^2. For each value of r_0, the three minima correspond to real volume integrals per nucleon J_v/A of about 360, 460, and 560 MeV fm^3, respectively.

In this expression $R_0 = r_0 A^{1/3}$, A is the target mass number, and A_p is the projectile mass number (3 for tritons). The χ^2 minima for each r_0 are for values of J_v/A of about 360, 460, and 560 MeV fm^3 per nucleon. Since the χ^2 curves are plotted on a logarithmic scale, the minima are much sharper than they appear in Fig. 8. The analyzing-power minima are uniformly offset from the cross-section minima in the direction of increasing V_0. Since the χ_A^2 oscillations are much more pronounced than those for χ_σ^2, the analyzing-power angular distributions delimit the real parameters more precisely than do the cross-section data.

The effect of V_0 on the calculated angular distributions is illustrated in Fig. 4 where we show for ^{90}Zr the fit for the ZR1 parameters (solid curve) and a calculation with V_0 changed to 160 MeV (dashed curve). The smaller value is near the χ_σ^2 minimum for $r_0 = 1.20$ fm (see Fig. 8), and a noticeable improvement in the fit to σ/σ_R is observed. The phase of the analyzing-power angular distribution is shifted, however, and no adjustment of the imaginary or spin-orbit parameters in Eq. (1) can substantially improve the fit. The difference in the χ^2 values for the two calculations is pronounced, since $\chi_\sigma^2 = 4.8$ and $\chi_A^2 = 6.3$ for $V_0 = 165$ MeV, while for $V_0 = 160$ MeV, $\chi_\sigma^2 = 2.5$ and $\chi_A^2 = 60$. As shown also in Fig. 7, the standard OM parametrization seems unable to simultaneously optimize fits to both cross-section and analyzing-power data.

To see whether searches at the other minima located by the parameter grid would yield better fits than the ZR1 parameters, we made automatic searches starting at each of the χ_A^2 minima in Fig. 8. In most cases χ^2 values could be reduced from the grid-search values, but no better minimum than ZR1 was found, as Fig. 9 shows graphically. There seems to be a slight preference for the $J_v/A \approx 460$ MeV fm^3 family. Within this family one can see that $r_0 = 1.20$ fm produces a better fit to the analyzing power, while $r_0 = 1.16$ fm improves the fit to the cross section while only slightly worsening χ_T^2. (This is consistent with the FABB analysis[10] which showed a strong preference for $r_0 = 1.16$ fm in fitting cross-section data.) During these calculations the automatic search code varied parameters within a fairly narrow range, generally $\pm 10\%$, from the ZR1 starting values. It is therefore possible that more-extensive searches could produce somewhat different conclusions, and the results presented in Figs. 8 and 9 should provide useful starting points.

Calculations using the OM parameters of previous analyses also failed to produce better fits

to our data, even when the spin-orbit parameters were allowed to vary. Figure 10 shows three of these calculations for the ^{90}Zr data. For the parameters of FABB (Ref. 10) and MSG (Ref. 16) $\chi_\sigma^2 \geq 19$, perhaps because of the 3-MeV energy increase from the present data to those used in their analyses. For the BG (Ref. 18) parameters $\chi_\sigma^2 = 54$, considerably greater than one would expect, especially since the BG parameters are energy-dependent; the two sets of cross-section data used in the BG analysis, at 15 and 20 MeV, may have led to an unphysical energy or isospin dependence in the global parametrization. In particular, the BG value for W_v of about 28 MeV is too high. The failure of previous parametrizations to reproduce satisfactorily the analyzing-power data illustrates again the great sensitivity of the calculated analyzing powers to the real central potential parameters.

Most of the previous analyses of only differential cross section data have centered on the $J_v/A \approx 460$ MeV fm^3 family. Both BG and Nurzynski[17] used $r_0 = 1.20$ fm, although Nurzynski also found parameter sets with $r_0 = 1.25$ fm and sets in the $J_v/A \approx 360$ MeV fm^3 family. FABB (Ref. 10) stayed in the $J_v/A \approx 460$ MeV fm^3 family, but used r_0 values of 1.16 and 1.24 fm. They preferred the smaller radius parameter for DWBA calculations of transfer reactions. On the other hand, MSG preferred $V_0 \approx 125$ MeV and varied r_0 between 1.13 and 1.34 fm. Considering all these factors, and the results in Fig. 9, we decided to fix r_0 at 1.20 fm and keep $V_0 \approx 150$ MeV, roughly three times the nucleon well depth and consistent with the folding model, for the remainder of this analysis. Thus the ZR1 parameters, Eq. (4), became the starting point for investigation of the other target nuclei.

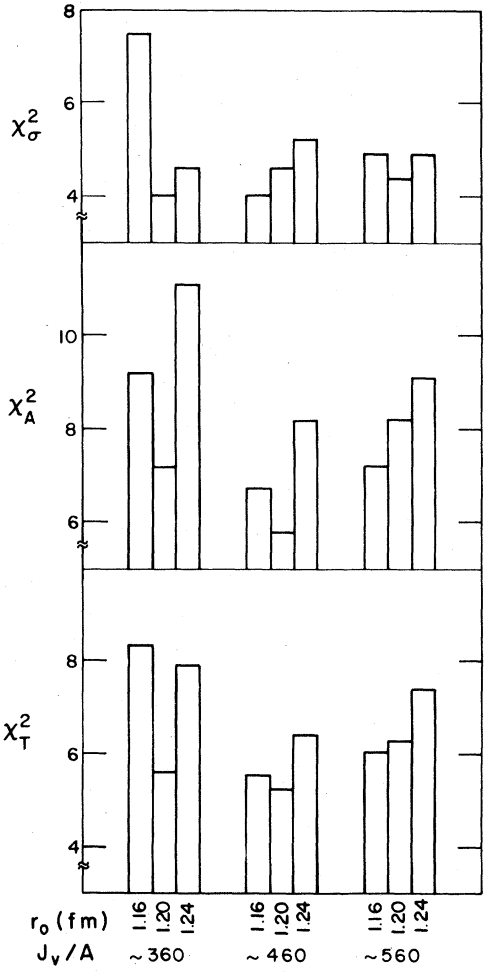

FIG. 9. The results for ^{90}Zr$(t,t)^{90}$Zr are summarized as bar graphs showing the best-fit χ^2 values resulting from automatic searches at the relative minima illustrated in Fig. 8. Except for r_0 and V_0, starting values for these searches were the ZR1 parameters, Eq. (4).

TABLE II. Optical-model potential parameters and χ^2 values for triton elastic scattering at 17 MeV. Fixed parameters are $r_0 = 1.20$ fm, $r_w = 1.60$ fm, $r_{so} = 1.10$ fm, $a_0 = 0.66$ fm, $r_C = 1.30$ fm.

Target	V_0 (MeV)	W_v (MeV)	a_w (fm)	V_{so} (MeV)	a_{so} (fm)	J_v/A (MeV fm^3)	χ_σ^2	χ_A^2	χ_T^2
^{40}Ca	163.0	18.6	0.82	6.0	0.45	494	44	98	71
^{46}Ti	154.0	21.6	0.95	4.0	0.60	458	36	34	35
^{48}Ti	167.0	20.0	0.71	8.1	0.40	494	30	29	30
^{54}Fe	157.0	18.8	0.74	6.7	0.66	458	10	6	8
^{56}Fe	153.0	17.6	0.85	7.0	0.66	444	7	19	13
^{58}Ni	151.0	18.2	0.83	4.0	0.83	437	11	10	10
^{60}Ni	146.0	18.3	0.89	7.5	0.77	421	13	31	22
^{68}Zn	170.0	18.0	1.00	7.5	0.77	484	30	38	34
^{90}Zr	165.0	13.8	0.80	6.0	0.40	457	4.8	6.3	5.5
^{94}Zr	160.5	14.0	0.95	3.5	0.40	443	3.2	8.2	5.7
^{116}Sn	151.5	14.5	1.00	8.0	0.80	411	4.4	6.4	5.4
^{140}Ce	162.0	13.4	0.99	6.0	0.80	434	4.3	0.9	2.6
^{208}Pb	160.0	11.0	1.08	6.0	0.98	419	1.8	1.8	1.8

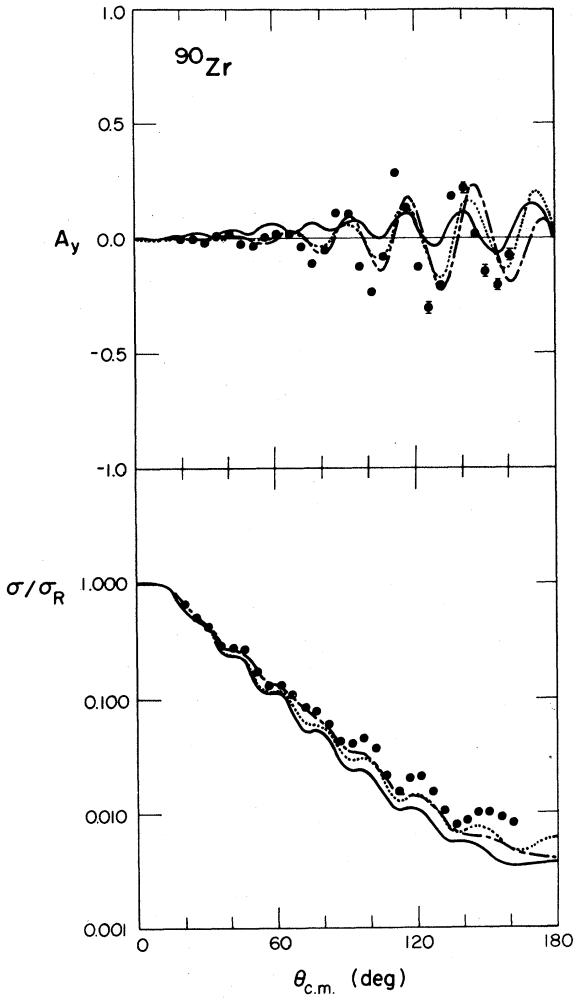

FIG. 10. The 17-MeV triton elastic scattering data for ^{90}Zr are shown with predictions from 20-MeV OM parametrizations of previous analyses: Becchetti and Greenlees (Ref. 18) (solid curve), Flynn *et al.* (Ref. 10) (short dash), and Mukhopadhyay, Srivastava, and Gunguly (Ref. 16) (short-long dash). All calculations use the ZR1 spin-orbit potential of the present analysis ($V_{so}=6.0$ MeV). In spite of this, it is seen that the calculated analyzing powers are uniformly too small in magnitude and out of phase with the data.

D. Analysis of other nuclei

The procedure for the OM analysis of the other target nuclei was similar to that for ^{90}Zr although not as comprehensive. The parameter searches for a given element (Z) started with the ZR1 parameters, while for isotopes, the searches usually started with parameters for the same Z. Fits were first optimized interactively in grid searches, then by automatic search, first varying the parameters to which χ_T^2 was most sensitive (usually V_0 and W_v for fixed geometry), then varying the less-sensitive parameters. As certain parameters showed little variation from nucleus to nucleus, or could be easily compensated by variation of other parameters, we tried to fix them at average values. Thus, we converged to fixed radii for the OM potentials, $r_0=1.20$ fm, $r_w=1.60$ fm, $r_{so}=1.10$ fm, and $r_c=1.30$ fm, in agreement with the ZR1 parameters [Eq. (4)].

Eventually, fits were constrained to $a_0=0.66$ fm when little variation between nuclei in this parameter was observed, and finally, an attempt was made to round some of the parameters to common values for other target nuclei when doing so did not make a significant difference in either χ_T^2 or the visual fit to the data. Except for V_0 and W_v, which were sensitive parameters for all of the nuclei, the sensitivity of the remaining parameters varied greatly from nucleus to nucleus. In particular, the fits were poor for the lighter nuclei (Fig. 1), and it was difficult to determine the parameters reliably. Hence, the results of this analysis, shown in Figs. 1–5 for the parameters in Table II, should be viewed as a reasonably thorough first attempt at delineating the spin-dependent OM for 17 MeV tritons. Slightly better fits to individual data sets were sometimes found when the geometric constraints were removed, but in no case were the improvements judged significant. Of course, if one has different goals, as in DWBA calculations for a particular target nucleus, the average parameters may not be as useful as a more specific parameter set.

E. Alternative parametrizations

Attempts were made in several cases to search for effects from other than the standard OM potential with volume absorption. We found no discernable improvement to the fits by using a surface absorption term,[17] either added to or replacing the volume absorption. We also tried modifying the radial form factor of the spin-orbit potential by changing the power of r in the denominator of Eq. (1), but no improvement in the fits resulted.

Recently, Goddard and Haeberli[25] reported improved results for deuteron scattering by including an imaginary spin-orbit term in the deuteron OM potential. In particular, this term seemed to move the oscillations of the cross section and analyzing powers into the same relative phase. Also, a strong-absorption-model analysis of helion data indicates a significant imaginary component in the spin-orbit potential.[26] We had tried an imaginary spin-orbit potential in our earlier 15-MeV analysis without noticeable

success,[5] and we tried it again in this work, but in only one case, ^{90}Zr, was there any significant improvement. An imaginary term with the same form factor as the real spin-orbit potential of Eq. (1), with $W_{so}=2.0$ MeV, $r_{wso}=1.20$ fm, and $a_{wso}=0.66$ fm, when added to a slightly modified ZR1 potential, gave $\chi_\sigma^2=1.5$ and $\chi_A^2=4.9$, compared with $\chi_\sigma^2=4.8$ and $\chi_A^2=6.3$ for the ZR1 parameters in Eq. (4). The major improvement came from reducing V_0 to 163.5 MeV, thus matching more closely the phase in cross-section oscillations, while keeping the analyzing-power phase matched by adjusting the imaginary spin-orbit potential. We could not duplicate these results for the other target nuclei with any combination of potential parameters. In a few cases the fits improved slightly, but the overall improvements were not significant.

V. DISCUSSION

A. Parameter variation with target mass

In Fig. 11 we show the OM potential depths (Table II) plotted as a function of target mass number. Although the number of targets investigated does not permit accurate interpolation, a certain pattern is suggested by our analysis. These possible trends are indicated in the figure by straight lines drawn as guides to the eye. One expects W to increase and/or V_0 to decrease as one moves away from a closed shell since additional absorption channels are open. Although there is no clear trend in our W_v values (except a slight decrease with mass number which may be caused by increasing Coulomb barrier), our V_0 values show a noticeable effect. The closed neutron shell nuclei ^{40}Ca, ^{90}Zr, ^{140}Ce, and ^{208}Pb have nearly equal well depths, while most of the collective nuclei have lower values. More data and analyses are clearly needed to explore this effect. Except for the BG energy- and isospin-dependent parametrization[18] which gives W_v values that are larger, the magnitude and trend of our results for W_v values agree roughly with previous analyses of 20-MeV cross-section data.[10,14-17] The spin-orbit potential is less well determined than the real and imaginary well depths, even though analyzing-power data were available. Nevertheless, a value near 6 MeV is acceptable, and we note that all of the closed-neutron-shell nuclei produce this value.

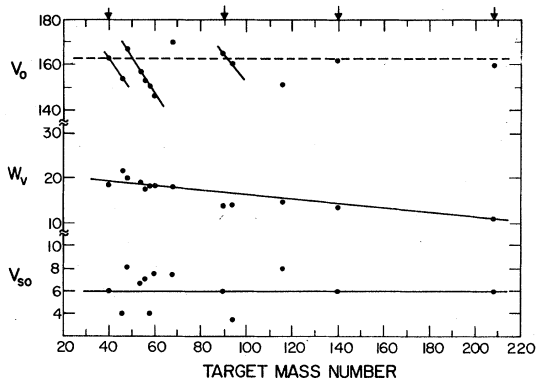

FIG. 11. The parameters from Table II for the well depths (MeV) of the real, volume imaginary, and spin-orbit OM potentials versus target mass number. Arrows at the top indicate those nuclei with a closed neutron shell. The solid lines are guides to the eye to suggest trends emerging from our analysis. The horizontal dashed line indicates an average value for V_0 of about 163 MeV for four nuclei with closed neutron shells. These four nuclei all have $V_{so}=6.0$ MeV, which is nearly the average value for all of the nuclei studied.

B. Applicability of the folding model

We discussed in IV B the failure of the simple folding model[19-22] to correctly predict the magnitude of the spin-orbit potential for triton scattering. To investigate this question further, and in a way which is insensitive to the particular form factors used for the scattering potentials, we consider appropriate integrals of the central and spin-orbit potentials. In folding models the volume integral (per projectile nucleon) over the real central potential

$$J_v=4\pi\int V_0 f(r, r_0, a_0) r^2 dr/A_p \tag{6}$$

can be written as[27]

$$J_v/A=J_0\pm J_1(N-Z)/A \tag{7}$$

with the isoscalar and isovector volume integrals, J_0 and J_1, respectively, independent of A_p and A and dependent only on the nucleon-nucleus interaction. In Eq. (7) the positive sign is appropriate for protons and ^{3}He, and the negative sign for neutrons and t. For the spin-orbit potential the radial integral calculated with an additional factor of r^2 (Ref. 27),

$$J_4=\int r^2 V_{so}\frac{2}{r}\frac{d}{dr}[f(r, r_{so}, a_{so})] r^2 dr/A\,, \tag{8}$$

depends only on the fraction f_{so} of the projectile nucleons which contribute to the spin-orbit coupling and on the nucleon-nucleus spin-orbit interaction. The folding model predicts that J_4/f_{so} should be independent of A_p and A. For the Woods-Saxon potential form factors used here, J_v/A was given in Eq. (5) for the real central potential, and

$$J_4 = 2V_{so}R_{so}^3[1+(\pi a_{so}/R_{so})^2]/A \quad (9)$$

for the spin-orbit potential where $R_{so}=r_{so}A^{1/3}$. Table III gives values of J_0, J_1, and J_4 for proton and mass-3 scattering. The (p,p) values are from the parametrization by Becchetti and Greenlees[1] and the folding-model analyses of (p,p) scattering by Greenlees, Makofske, and Pyle.[27] The large uncertainty in J_1 has been discussed by Hodgson.[28] The values of J_0 and J_1 for ^{3}He scattering were obtained from eight OM analyses in the energy range 15 to 20 MeV for targets $40 \leq A \leq 124$, as tabulated in the survey by Perey and Perey,[29] then making a least-squares fit to J_0 and J_1 in Eq. (7). The spin-orbit integrals J_4 were obtained from analyses of ^{3}He elastic-scattering polarization and analyzing power measurements[4,30] in the energy range 18 to 33 MeV for targets with $9 \leq A \leq 58$, a total of 10 sets of data. For triton scattering two sets of parameters were used. The first set, for the real central potential only, was from the tabulation by Perey and Perey[29] for energies in the range 15 to 20 MeV for targets with $54 \leq A \leq 207$, a total of 18 energies and targets. The second parameter set was from the present experiment, 13 targets with $40 \leq A \leq 208$ at 17 MeV.

For the isoscalar real central volume integral J_0 there is consistency for the three projectiles. The isovector integral J_1 is difficult to extract, partly because of the small range of $(N-Z)/A$ available, and partly because its extraction depends on knowing the energy dependence of the potentials.[28] For ^{3}He J_1 is anomalous, since it is expected to be the same as for p and t. This discrepancy has been seen previously,[31] and may be attributed to the large error associated with the J_1 values.

The spin-orbit integrals J_4/f_{so} should be the same for all targets and for all projectiles according to the folding model. The target independence is here established within the ~30% uncertainty in extracting J_4. However, J_4/f_{so} is about 3 times larger for ^{3}He and t than for proton scattering, as if all three nucleons rather than a single nucleon were participating in the spin-orbit interaction. This general result is more significant than the failure of the folding model to fit a given analyzing-power angular distribution, as in Fig. 1 of Ref. 5. Further, the values of J_4 do not discriminate between the spin-orbit potentials having the unusually small values of a_{so} found in the analysis of polarized-^{3}He elastic scattering[4] and the value $a_{so} \geq 0.40$ fm determined here for t scattering.

TABLE III. Volume integrals per nucleon estimated as described in Sec. V B. The units of J_0 and J_1, which are defined in Eq. (7), are MeV fm^3, and those of J_4 are MeV fm^5. The uncertainties are standard deviations from least-squares fits as a function of target mass number. The value of f_{so} is that assumed in simple folding models of the spin-orbit interaction.

Projectile	J_0	J_1	f_{so}	J_4/f_{so}
p	435 ± 35	$180 \pm \frac{180}{360}$	1	17 ± 2
^{3}He	470 ± 30	−210 ± 220	$\frac{1}{3}$	48 ± 18
t [a]	490 ± 10	220 ± 60		
t [b]	460 ± 15	260 ± 120	$\frac{1}{3}$	60 ± 15

[a] Using Ref. 29. [b] Present work.

C. Summary

The data presented in this paper provide the first opportunity to study the spin-dependent optical model for mass-3 projectiles over a wide range of targets. After exploring the discrete ambiguities from increasing values of the real volume integral J_v, we concentrated on the family with $J_v/A \approx 460$ MeV fm^3 and fixed the real well radius at 1.20 fm. The resulting searches and parameter averaging led to the potentials of Table II in which all the radii and the real well diffuseness a_0 were fixed. Fits to the data were acceptable for the heavier nuclei ($A \geq 90$) but only fair for the lighter nuclei studied. The values of V_0 seem to suggest a pattern when plotted against target mass number (Fig. 11), but more data and analyses are needed to confirm this trend.

Polarization effects for triton scattering are much larger than expected from the simple folding model, confirming preliminary findings[5] at 15 MeV. The magnitude of the spin-orbit potential V_{so} is only determined, however, by fitting both the differential-cross-section and analyzing-power data together, since the central potential has a strong effect on the analyzing-power calculation. Our analysis has not resulted in a unique value for V_{so}, but for the geometries listed the average (with standard deviation) of the well depths in Table II is $V_{so}=6.2\pm1.5$ MeV. This should be used with the values found for the imaginary potentials which range from near 20 MeV for ^{40}Ca to 11 MeV for ^{208}Pb. Even though a reasonable fit to A_y alone can sometimes be achieved with $V_{so} \approx 2.5$ MeV (Ref. 32), our analysis strongly supports V_{so} between 4 and 8 MeV if both differential-cross-section and polarization effects are to be correctly predicted.

It is emphasized that the fits to the present data result from a compromise between optimum fits to the cross-section and analyzing-power data.

This compromise generally favors the analyzing-power data because of the increased sensitivity of this observable to the OM parameters, but the failure to fit both cross section and analyzing-power simultaneously must be viewed as a failure of the standard OM to correctly describe the interaction. Additional terms in the potential appear to be needed, and we have briefly investigated two possibilities, a surface absorption term, which made no improvement, and an imaginary spin-orbit potential, which gave significantly improved results only for ^{90}Zr.

ACKNOWLEDGMENTS

The authors gratefully acknowledge the assistance of L. J. Morrison with the operation of the polarized triton source and J. M. Gursky, who provided many of the targets. The cooperation of R. V. Poore was very helpful in getting the interactive computer code running, and discussions with E. R. Flynn were useful during the data analysis. This work was performed under the auspices of the U. S. Department of Energy.

---

*Permanent address: Department of Physics and Astronomy, University of North Carolina, Chapel Hill, NC 27514.

[1]F. G. Perey, Phys. Rev. 131, 745 (1963); F. D. Becchetti and G. W. Greenlees, *ibid.* 182, 1190 (1969).
[2]O. Karban, S. Oh, and W. B. Powell, Phys. Rev. Lett. 33, 1438 (1973).
[3]R. A. Hardekopf, in *Proceedings of the Fourth International Symposium on Polarization Phenomena in Nuclear Reactions, Zürich, 1975,* edited by W. Grüebler and V. König (Birkhâser, Basel, 1976), p. 865.
[4]S. Roman, A. K. Basak, J. B. A. England, O. Karban, G. C. Morrison, and J. M. Nelson, Nucl. Phys. A284, 365 (1977); O. Karban, W. E. Burcham, J. B. A. England, R. G. Harris, and S. Roman, *ibid.* A292, 1 (1977).
[5]R. A. Hardekopf, L. R. Veeser, and P. W. Keaton, Jr., Phys. Rev. Lett. 35, 1623 (1975).
[6]P. A. Schmelzbach, R. A. Hardekopf, R. F. Haglund, Jr., and G. G. Ohlsen, Phys. Rev. C 17, 16 (1978).
[7]G. G. Ohlsen and P. A. Lovoi, in *Proceedings of the Fourth International Symposium on Polarization Phenomena in Nuclear Reactions, Zürich, 1975* (see Ref. 3), p. 907.
[8]R. A. Hardekopf, G. G. Ohlsen, R. V. Poore, and Nelson Jarmie, Phys. Rev. C 13, 2127 (1976).
[9]G. G. Ohlsen and P. W. Keaton, Jr., Nucl. Instrum. Methods 109, 41 (1973).
[10]E. R. Flynn, D. D. Armstrong, J. G. Berry, and A. G. Blair, Phys. Rev. 182, 1113 (1969).
[11]R. J. Eastgate, W. J. Thompson, and R. A. Hardekopf, Comput. Phys. Commun. 5, 69 (1973).
[12]P. Schwandt, Indiana University (unpublished).
[13]R. N. Glover and A. D. W. Jones, Nucl. Phys. 81, 268 (1966).
[14]J. C. Hafele, E. R. Flynn, and A. G. Blair, Phys. Rev. 155, 1238 (1967).
[15]P. P. Urone, L. W. Put, H. H. Chang, and B. W. Ridley, Nucl. Phys. A163, 225 (1971).
[16]S. Mukhopadhyay, D. K. Srivastava, and N. K. Ganguly, Nucl. Phys. A257, 264 (1976).
[17]J. Nurzynski, Nucl. Phys. A246, 333 (1975).
[18]F. D. Becchetti, Jr., and G. W. Greenlees, in *Proceedings of the Third International Symposium on Polarization Phenomena in Nuclear Reactions*, edited by H. Barschall and W. Haeberli (Univ. of Wisconsin Press, Madison, Wisconsin, 1970), p. 682; F. D. Becchetti, W. Makofske, and G. W. Greenlees, Nucl. Phys. A190, 437 (1972).
[19]S. Watanabe, Nucl. Phys. 8, 484 (1958).
[20]A. Y. Abul-Magd and M. El-Nadi, Prog. Theor. Phys. 35, 798 (1966).
[21]P. W. Keaton, Jr., E. Aufdembrink, and L. R. Veeser, Los Alamos Scientific Laboratory Report No. LA-4379-MS, 1970 (unpublished).
[22]P. W. Keaton, Jr., in *Proceedings of the Fourth International Symposium on Polarization Phenomena in Nuclear Reactions, Zürich, 1975* (see Ref. 3), p. 173.
[23]J. R. Shepard and J. J. Kraushaar, University of Colorado NPL Tech. Progress Report, 1976 (unpublished), p. 70.
[24]G. W. Greenlees, G. J Pyle, and Y. C. Tang, Phys. Rev. 171, 1115 (1968).
[25]R. P. Goddard and W. Haeberli, Phys. Rev. Lett. 40, 701 (1978).
[26]T. F. Hill and W. E. Frahn, Ann. Phys. (N.Y.) (to be published).
[27]G. W. Greenlees, W. Makofske, and G. J. Pyle, Phys. Rev. C 1, 1145 (1970).
[28]P. E. Hodgson, Nucl. Phys. A150, 1 (1970).
[29]C. M. Perey and F. G. Perey, At. Data Nucl. Data Tables 17, 1 (1976).
[30]W. S. McEver *et al.*, Nucl. Phys. A178, 529 (1972); W. E. Burcham *et al.*, *ibid.* A246, 269 (1975); M. D. Cohler *et al.*, J. Phys. G 2, L151 (1976).
[31]P. P. Urone *et al.*, Nucl. Phys. A167, 383 (1971).
[32]S. Mordechai and H. T. Fortune, J. Phys. G 4, L177 (1978).